PROCEEDINGS, 44th Workshop on Geothermal Reservoir Engineering
Stanford University, Stanford, California, February 11-13, 2019
SGP-TR-214

A Numerical Scheme to Reduce Numerical Diffusion for Advection-Dispersion Modeling: Validation and Application

Hui Wu, Pengcheng Fu, Joseph P. Morris, Randolph R. Settgast, Frederick J. Ryerson and EGS Collab Team[1]

Atmospheric, Earth, and Energy Division, Lawrence Livermore National Laboratory, Livermore, CA 94550

Corresponding E-mail address: wu40@llnl.gov

Keywords: Advection-dispersion, numerical scheme, numerical diffusion, analytical solution, EGS

ABSTRACT

Advection-dispersion is an essential process in most fluid dynamics problems such as tracer test for reservoir characterization. Many numerical schemes have been developed to simulate this process. However, numerical diffusion encountered in these schemes causes inaccuracy in simulation results, and efforts to reduce numerical diffusion usually lead to other problems such as instability of schemes and oscillation in results. We present a new scheme, named Intra-Cell Advection Tracking (ICAT), to minimize numerical diffusion as well as preserve stability and monotonicity for advection-dispersion modeling. In this new scheme, the key idea is to track scalar transport in each discretized cell by introducing a queue in this cell to connect the inflow and outflow interfaces. We use a sequential transport rule to temporally track the scalar transport in the queue, and use a flow distribution mechanism to spatially track the scalar transport among queues in different cells. Two test cases are performed to investigate the capability of ICAT. Compared with the results obtained from other numerical schemes, the results from ICAT have less numerical diffusion and agree better with analytical solutions. We also employ ICAT to simulate the transport process of a conservative tracer in a fracture with a highly heterogeneous aperture distribution. Discrete flow channels in the fracture are better discerned by ICAT than by other numerical schemes, indicating the suitability of ICAT for modeling tracer transport in channelized flow fields.

1. INTRODUCTION

Advection-dispersion is a ubiquitous phenomenon in many fluid dynamics problems such as climate change, contaminant transport, subsurface reservoir characterization, drug delivery and so on (Patankar, 1980; Tang et al., 1981; Marshall et al., 2006; Pontrelli and de Monte, 2007; Versteeg and Malalasekera, 2007; Calo et al., 2008; Kumar et al., 2010; Hawkins et al., 2017). Both analytical solutions and numerical simulations have been employed to analyze the transport of certain scalars (such as heat and mass) in advection-dispersion process. Since analytical solutions are only applicable to a limited number of idealized scenarios, much effort has been devoted to developing numerical schemes to simulate the advection-dispersion process in arbitrary flow fields.

A main consideration for developing a robust numerical scheme is the trade-off between the accuracy of the results and the stability of the scheme. Low-order schemes such as the upstream difference scheme (UDS) is stable under various flow conditions but suffers from severe numerical diffusion caused by truncation error and flow field-to-grid skewness, while high-order schemes such as the central difference scheme (CDS) has less severe numerical diffusion but may become unstable when the Peclet number is greater than 2, and the results may have oscillations (Leonard, 1979; Rood, 1987; Arampatzis and Assimacopoulos, 1994). For example, the leapfrog scheme is second-order accurate in time, and compared with UDS, it has less severe numerical diffusion but always shoes undesired oscillations in the results (Courant et al., 1928). The Lax-Wendroff scheme introduces a diffusion term to stabilize CDS under high Peclet number conditions, and as a side effect, leads to oscillation (Lax, 1954; Lax and Wendroff, 1960). The Quadratic Upstream Interpolation for Convective Kinematics (QUICK) scheme and QUICKEST scheme employ a quadratic interpolation method which involves more neighboring cells to estimate the advection term at a cell interface. The results from QUICK and QUICKEST are less numerical diffusive but may have oscillations with unphysically high and negative values (Leonard, 1979). The Flux-Corrected Transport (FCT) scheme preserves monotonicity in the solution by combing the accurate, high-order but dispersive scheme with the low-order, monotonic but diffusive scheme. However, although considerably less diffusive than the results from UDS, the results from FCT still contain scale-dependent diffusion (van Leer, 1977; Roe, 1986; Brasseur and Jacob, 2017). The Multidimensional Positive-Definite Advection Transport

[1] J. Ajo-Franklin, S.J. Bauer, T. Baumgartner, K. Beckers, D. Blankenship, A. Bonneville, L. Boyd, S.T. Brown, J.A. Burghardt, T. Chen, Y. Chen, K. Condon, P.J. Cook, P.F. Dobson, T. Doe, C.A. Doughty, D. Elsworth, J. Feldman, A. Foris, L.P. Frash, Z. Frone, P. Fu, K. Gao, A. Ghassemi, H. Gudmundsdottir, Y. Guglielmi, G. Guthrie, B. Haimson, A. Hawkins, J. Heise, C.G. Herrick, M. Horn, R.N. Horne, J. Horner, M. Hu, H. Huang, L. Huang, K. Im, M. Ingraham, T.C. Johnson, B. Johnston, S. Karra, K. Kim, D.K. King, T. Kneafsey, H. Knox, J. Knox, D. Kumar, K. Kutun, M. Lee, K. Li, R. Lopez, M. Maceira, N. Makedonska, C. Marone, E. Mattson, M.W. McClure, J. McLennan, T. McLing, R.J. Mellors, E. Metcalfe, J. Miskimins, J.P. Morris, S. Nakagawa, G. Neupane, G. Newman, A. Nieto, C.M. Oldenburg, W. Pan, R. Pawar, P. Petrov, B. Pietzyk, R. Podgorney, Y. Polsky, S. Porse, S. Richard, B.Q. Roberts, M. Robertson, W. Roggenthen, J. Rutqvist, D. Rynders, H. Santos-Villalobos, M. Schoenball, P. Schwering, V. Sesetty, A. Singh, M.M. Smith, H. Sone, C.E. Strickland, J. Su, C. Ulrich, N. Uzunlar, A. Vachaparampil, C.A. Valladao, W. Vandermeer, G. Vandine, D. Vardiman, V.R. Vermeul, J.L. Wagoner, H.F. Wang, J. Weers, J. White, M.D. White, P. Winterfeld, T. Wood, H. Wu, Y.S. Wu, Y. Wu, Y. Zhang, Y.Q. Zhang, J. Zhou, Q. Zhou, M.D. Zoback

Algorithm (MPDATA) uses an iterative approach based on UDS to reduce numerical diffusion but the solution is not free from oscillations under shock-type initial conditions (Smolarkiewicz, 1984).

In this study, a new scheme, named Intra-Cell Advection Tracking (ICAT), is developed in the UDS framework to minimize numerical diffusion as well as to preserve stability and monotonicity for advection-dispersion modeling. The key idea is to track scalar transport in each discretized cell temporally and spatially using "queues". The mechanism of ICAT under one-dimensional (1D) and multidimensional conditions is first illustrated. Two test cases are then performed to validate the effectiveness of ICAT. The first test case examines the transport of a conservative tracer in a 1D model with a pulse-type injection where the effects of the Courant number and the Peclet number are analyzed. The second test case assumes a uniform but skew-to-grid flow field in a two-dimensional (2D) model. A more realistic model involving the transport of a conservative tracer in a rock fracture is developed to study the potential application of ICAT to identify discrete flow channels in unconventional reservoirs.

2. MECHANISM OF ICAT

2.1 ICAT scheme under 1D condition

Consider the advection and dispersion of a scalar ϕ in a 1D model (Fig. 1(a)). The governing equation to be solved is the continuity equation for this scalar

$$\frac{\partial \phi}{\partial t} = -\frac{\partial (v_x \phi)}{\partial x} + \frac{\partial}{\partial x}\left(D \frac{\partial \phi}{\partial x}\right) \qquad (1)$$

where t is time; v_x is the flow velocity; D is the hydrodynamic dispersion coefficient. Using the finite volume method, the computational domain is discretized into non-overlapping cells. In each cell, integrating equation (1) over the cell and applying the divergence theorem yields

$$\int_\Omega \frac{\partial \phi}{\partial t} dV = -\int_\Gamma u\phi \cdot \mathbf{n} d\Gamma + \int_\Gamma D \frac{\partial \phi}{\partial x} \cdot \mathbf{n} d\Gamma \qquad (2)$$

where Ω is the volume and Γ is the boundary of the volume; $\mathbf{n}$ is the unit normal to the boundary. Consider cell i in Fig. 1(a), equation (2) can be expressed as

$$\phi_i(t+\Delta t) - \phi_i(t) = -\frac{u\Delta t}{\Delta x}[\phi_{i+1/2}(t) - \phi_{i-1/2}(t)] + \frac{D\Delta t}{\Delta x^2}[\phi_{i+1}(t) - 2\phi_i(t) + \phi_{i-1}(t)] \qquad (3)$$

where Δt is the time step and Δx is the cell length; the subscript i–1/2 and i+1/2 denote the interfaces between the three cells. To calculate $\phi_i(t+\Delta t)$, we need to use the scalar values at the upstream and downstream faces of cell i, i.e., $\phi_{i-1/2}(t)$ and $\phi_{i+1/2}(t)$. UDS assumes that the scalar distribution is uniform in each cell and therefore $\phi_{i-1/2}(t) = \phi_{i-1}(t)$and $\phi_{i+1/2}(t) = \phi_i(t)$. For a 1D advection-dispersion problem, numerical diffusion is mainly caused by the incorrect estimation of advection terms at the interfaces between discretized cells (truncation error). Assume that $D = 0$ and the Courant number c (= $v_x\Delta t/\Delta x$) is 0.5. At t_0, the scalar value is ϕ_0 in cell (i-1) and zero in cells i and (i+1), and in each time step, the scalar moves half of the cell length under advection (Fig. 1(b)). For UDS, at $t_0+\Delta t$, the scalar values at the upstream and downstream faces of cell i are estimated to be $0.5\phi_0$ (Fig. 1(c)), while the true values are ϕ_0 and 0 (Fig. 1(b)).

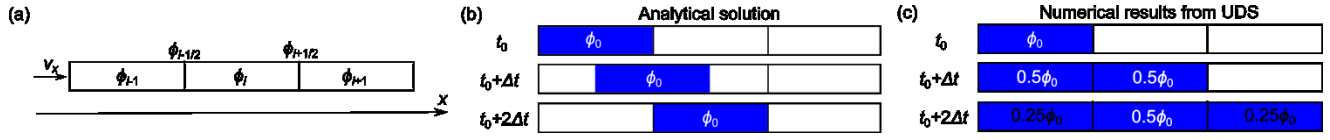

Figure 1: The generation of numerical diffusion in UDS in a 1D advection problem. (a) A 1D advection model with a constant flow field. The value annotated in each cell is the average scalar value in the cell. (b) Analytical solution for scalar transport when the Courant number = 0.5. (c) Numerical results from UDS when the Courant number = 0.5.

As shown in Fig. 1(c), UDS smears the scalar into a single value in the entire cell and the scalar front instantaneously moves to the downstream interface of the cell, causing the incorrect estimate of the scalar values at the cell interfaces. A key to reduce such numerical diffusion is therefore to track the scalar transport within each cell. In the proposed ICAT scheme, we introduce a "queue" in each cell to connect the upstream interface and the downstream interface and use a sequential transport rule to track the scalar transport along the queue. For a cell e, the queue contains N_e "queue-cells"

$$N_e = \left\lceil \frac{V_e}{q_e \Delta t} \right\rceil \qquad (4)$$

where V_e is the volume of cell e; q_e is the flow rate in cell e, and $\lceil\ \rceil$ is the rounding-up operator. For the 1D model in Fig. 1, N_e also equals $\lceil 1/c_e \rceil$, where c_e is the Courant number of cell e. As ICAT is still a variant of UDS, it also requires that the Courant number for each cell is not greater than one, implying that N_e is no less than one. Each queue-cell has two attributes: the volume, which is a constant, and the scalar value that evolves with the advection-dispersion process. The queue volume (the sum of all the queue-cell volumes) equals the volume of the host cell, and the scalar value of the host cell, when such "upscaled" quantity is needed, can be calculated as the average of the scalar values in the queue-cells weighted by the queue-cell volumes. Consider a general 1D scenario that the computational domain is discretized into cells with different volumes and $V_e/(q_e\Delta t)$ is not necessarily an integer for every cell (Fig. 2(a)). The queue-cell volumes

are calculated as: The volume of the first queue-cell (closest to the upstream interface) is $V_e^1 = V_e - (N_e - 1)q\Delta t$, and all the other queue-cells have a volume of $q\Delta t$ so that the scalar front moves one queue-cell length in each time step in these queue-cells. Since N_e is the smallest integer greater than $V_e/(q_e\Delta t)$, V_e^1 is smaller than $q\Delta t$. The fluid entering cell e would fill the first queue-cell in entirety and partially fill the second queue-cell (Fig. 2(a)). The proportion of the scalar transporting to the first queue-cell, α_e, is the ratio between the volume of the first queue-cell and the volume of the fluid entering the cell in one time step, i.e., $\alpha_e = [V_e - (N_e - 1)q\Delta t]/(q\Delta t)$. In the queue, the scalar is essentially represented by a piecewise-constant function, and transports downstream along the queue accordingly. The physical dispersion in ICAT is handled in the same way as that in UDS, that the physical dispersion only occurs between neighboring cells and there is no physical dispersion among the queue-cells. In each time step, we first calculate the physical dispersion term and update the scalar values in queues, and then apply the sequential transport rule to calculate the advection term.

We use two examples to show how ICAT works in 1D (Fig. 2(b) and (c)). The physical dispersion is ignored. The initial condition and flow field are the same as that in Fig. 1(c). In the first example, $V_e/(q_e\Delta t) = 2$ is the same for all the cells (Fig. 2(b)), and therefore each cell has a queue with two queue-cells. In each time step, the scalar travels exactly one queue-cell length and no numerical diffusion is generated. In the second example, $V_e/(q_e\Delta t)$ is 2, 2.7 and 1.3 for the three cells, respectively. According to the sequential transport rule, we calculate the scalar distribution after Δt, $2\Delta t$, and $3\Delta t$ (Fig. 2(c). Numerical diffusion occurs but is less severe than that in UDS (Fig. 2(c) vs. Fig. 1(d)).

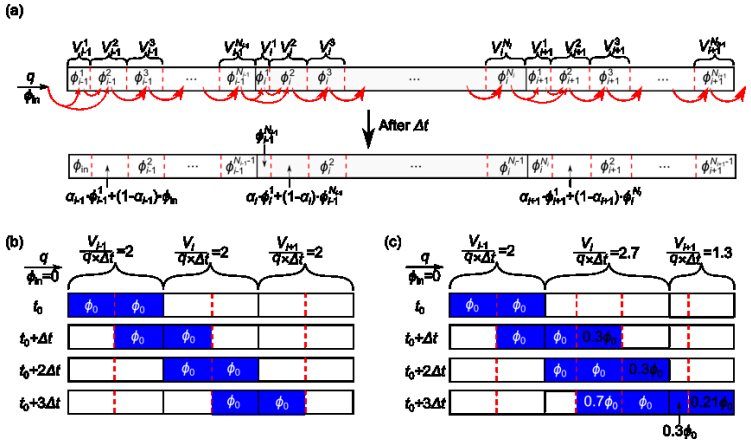

Figure 2: The operations of ICAT in 1D example problems. (a) The sequential transport rule for the 1D problem. The red dash lines divide a cell into queue-cells. ϕ_{in} is the scalar value in the fluid flowing into cell (i–1). V_e^m and ϕ_e^m (m = 1, 2, … N_e) are the volume of the queue-cell and the scalar value in this queue-cell, respectively. The red arrows denote the scalar transport within each cell and between neighboring cells. (b) An example showing how ICAT works for a simple scenario with $V_e/(q_e\Delta t)$ = 2 for all cells. (c) An example showing how ICAT works for a general scenario that $V_e/(q_e\Delta t)$ is 2, 2.7 and 1.3 for cell (i–1), i and (i+1), respectively.

2.2 ICAT scheme under multidimensional condition

In a multidimensional problem (2D or 3D), numerical diffusion originates from not only the truncation error but also the flow field-to-grid skewness. A cell may have multiple inflow faces and multiple outflow faces, and scalars entering the cell through different inflow faces are smeared if they flow into the same queue-cell. An intra-cell queue, which is essentially a 1D construct, and the associated sequential transport rule cannot spatially track the scalar transport in this scenario. In order to further reduce the numerical diffusion caused by flow field-to-grid skewness, we attach a queue to each inflow face of a given cell to separately track the scalar entering the cell in different directions (Fig. 3(a)). As multiple inflow and outflow faces are involved, we need to determine the allocation of fluid from each intra-cell queue to the multiple outflow faces of the same cell. In a cell with m_{in} inflow faces and m_{out} outflow faces, there are $m_{\text{in}} \times m_{\text{out}}$ possible combinations of inflow-outflow pairs. We introduce a heuristic flow distribution mechanism to allocate the fluid flow among these pairs by prioritizing the pairs that imply flow directions that are more consistent with the overall flow velocity of this cell.

Consider a cell with two inflow faces and two outflow faces (Fig. 3(a)). Each inflow face has a queue, and the length of the queue is calculated by the following equation

$$V_{i\_f} = \frac{q_{i\_f} V_i}{\sum_{g=1}^{g=m_{in}} q_{i\_g}} \quad N_{i\_f} = \left\lceil \frac{V_{i\_f}}{q_{i\_f}\Delta t} \right\rceil \qquad (5)$$

where V_{i_f} and N_{i_f} are the total volume and the length of the queue attached to the f_{th} inflow face of cell i, respectively; q_{i_f} is the flow rate at the inflow face; m_{in} is the number of inflow faces in cell i. Note that in a 1D scenario, there is only one queue in each cell, and the queue volume equals the volume of the cell. In this 2D case, the cell has two queues, and the volume of the cell is distributed between the two queues in proportion to flow rates through the two corresponding interfaces. The volumes of queue-cells in each queue are then calculated in the same way as that introduced for 1D. Within each queue, the scalar transport can be simplified to a 1D problem and be tracked using the sequential transport rule. Note that equation (5) dictates that the two queues in cell i in Fig. 3(a) have the same length ($N_{i\_1} = N_{i\_2}$).

Now we introduce the flow distribution mechanism for flow allocation among different inflow-outflow pairs. For cell i, we first approximate the overall flow velocity vector of cell i ($\mathbf{v}_i$) as

$$\mathbf{v}_i = \sum_{f=1}^{m_{in}+m_{out}} \mathbf{v}_{i\_f}/2 \quad (6)$$

where $\mathbf{v}_{i\_f}$ is the flow velocity at the f_{th} face in cell i. As mentioned before, the inflow-outflow pair that implies a flow direction that are most consistent with the overall flow velocity has the highest priority in the fluid allocation. For each inflow-outflow pair, we calculate the angle between the implied flow direction and the overall flow velocity as the priority factor for this pair

$$\theta_{i\_a-b} = \cos^{-1}\left[\frac{\mathbf{v}_i \cdot (\mathbf{v}_{i\_a}+\mathbf{v}_{i\_b})}{\|\mathbf{v}_i\| \cdot \|\mathbf{v}_{i\_a}+\mathbf{v}_{i\_b}\|}\right] \quad (7)$$

where $\mathbf{v}_{i\_a}$ and $\mathbf{v}_{i\_b}$ denote the flow velocities at the inflow face a and the outflow face b, respectively. We compute θ for all the pairs and sort the pairs in an ascending order of θ. The allocation proceeds going down the list. For each inflow-outflow pair, we allocate the smaller of (1) the remaining inflow rate to be allocated on the inflow face in the pair and (2) the remaining outflow rate on the outflow face in the pair to the inflow-outflow pair. We then subtract the allocated amount from both the inflow and outflow rates on the two faces before processing the next pair in the sorted list. When an inflow face is depleted or an outflow face is full, we remove all the pairs that involve the inflow face or outflow face from the list. Due to the mass conservation condition in each cell, this process completes when all the inflow faces are depleted and all the outflow faces are filled.

We use an example to show the fluid allocation in the 2D cell in Fig. 3(a). Assume that the flow field is uniform ($\mathbf{v}_{i\_1} = \mathbf{v}_{i\_3}$, $\mathbf{v}_{i\_2} = \mathbf{v}_{i\_4}$) with $\|\mathbf{v}_{i\_1}\| > \|\mathbf{v}_{i\_2}\|$, and that cell is square, meaning that $q_{i\_1} = q_{i\_3} > q_{i\_2} = q_{i\_4}$. According to the above flow distribution mechanism, the priority factors of the four inflow-outflow pairs are sorted as $\theta_{i\_1\text{-}4} = \theta_{i\_2\text{-}3} = 0 < \theta_{i\_1\text{-}3} = \theta_{i\_2\text{-}4}$. The fluid/scalar at face 1 first flows out of the cell through face 4, and the fluid/scalar at face 2 flows out of the cell through face 3. Since $\|\mathbf{q}_{i,1}\| > \|\mathbf{q}_{i,4}\|$, the flow rate from face 1 to face 4 is $\|\mathbf{q}_{i,4}\|$, and the rest ($\|\mathbf{q}_{i,1}\| - \|\mathbf{q}_{i,4}\|$) will flow to face 3. The flow rate from face 2 to face 4 is zero since $\|\mathbf{q}_{i,2}\| < \|\mathbf{q}_{i,3}\|$. As a result, the scalar value at face 4 is $\phi_{i\_1}^{N_{i\_1}}$. Since face 3 receives fluid/scalar from both face 1 ($q_{i\_1} - q_{i\_4}$) and face 2 (q_{i_2}), the scalar value at face 3 is therefore equal to $w\phi_{i\_1}^{N_{i\_1}} + (1-w)\phi_{i\_2}^{N_{i\_2}}$, where $w = (q_{i\_1} - q_{i\_4})/q_{i\_3}$.

Fig. 3(b) shows the track of scalar in ICAT for a 2D problem. At t_0, the scalar value is ϕ_0 in cell i and zero in other cells. According to the flow distribution mechanism, the scalar from the queue attached on face 1 will flow to face 4 and that from the queue attached on face 2 will flow to face 3. According to the sequential transport rule, the scalar moves one queue-cell length in each queue in one time-step. After four time-steps, the scalar in cell i flows to cell l.

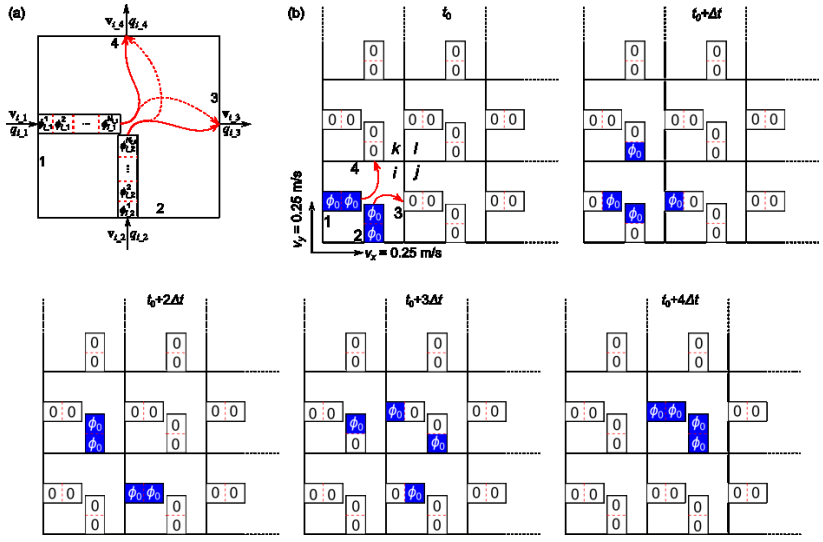

Figure 3: The operations of ICAT under 2D conditions. (a) Flow distribution mechanism in a 2D cell with two inflow faces and two outflow faces. Two queues are attached on the two inflow faces (1 and 2) respectively. The red arrow lines describe the four possible flow directions. The occurrence of the flow depicted by the two dash red arrow lines depends on the relationship between q_{i_1}, q_{i_2}, q_{i_3} and q_{i_4}. (b) An example of ICAT in a 2D domain discretized into 1 m × 1 m cells. i, j, k and l are cell indices. The velocity magnitude is 0.25 m/s in both the horizontal and vertical directions, and Δt is 1 s.

3. VALIDATION OF ICAT

In this section, we use three test cases to analyze the capability and limitations of ICAT. The results from ICAT are compared with both analytical solutions and numerical results from other commonly used schemes such as UDS and QUICK.

3.1 Transport of a conservative tracer in a 1D model

In this test case, a conservative tracer is injected into a 1D model and we use different numerical schemes to model the tracer transport (Fig. 5(a)). Since the tracer is conservative, we only consider advection and dispersion of the tracer in the 1D model.

First, we study the tracer transport in an advection-only scenario ($D = 0$). Fig. 5(b) shows the evolution of relative concentration (ϕ/ϕ_0) at point A obtained from the analytical solution and different numerical schemes. Since the Courant number c is smaller than 1, numerical diffusion is significant in the results from UDS. For ICAT, the results are the same as the analytical solution if $1/c$ is an integer and show slight numerical diffusion otherwise. Second, physical dispersion is considered and the effect of the Peclet number P_e ($= v_x\Delta x/D$) is analyzed (Fig. 5(c)). The analytical solution is derived by assuming a semi-infinite domain with zero initial concentration and applying the first-type inlet condition at the injection boundary (Gross et al., 1999)

$$\phi(x,t) = \begin{cases} \phi_0 A(x,t) & 0 < t \le t_0 \\ \phi_0[A(x,t) - A(x,t-t_0)] & t > t_0 \end{cases} \quad (8)$$

$$A(x,t) = \frac{1}{2}\mathrm{erfc}\left[\frac{x-v_x t}{\sqrt{4Dt}}\right] + \frac{1}{2}\exp\left(\frac{v_x x}{D}\right)\mathrm{erfc}\left[\frac{x+v_x t}{\sqrt{4Dt}}\right] \quad (9)$$

where t_0 is the injection time. Under a high Peclet number condition ($P_e = 5$), the results from UDS suffer a significant numerical diffusion, while that from ICAT agree well with the analytical solution. For a low Peclet number condition ($P_e = 0.5$), the results from the two numerical schemes are almost the same and all coincide with the analytical solution. UDS is suitable for the low Peclet number condition, while ICAT can be used for both high and low Peclet number conditions.

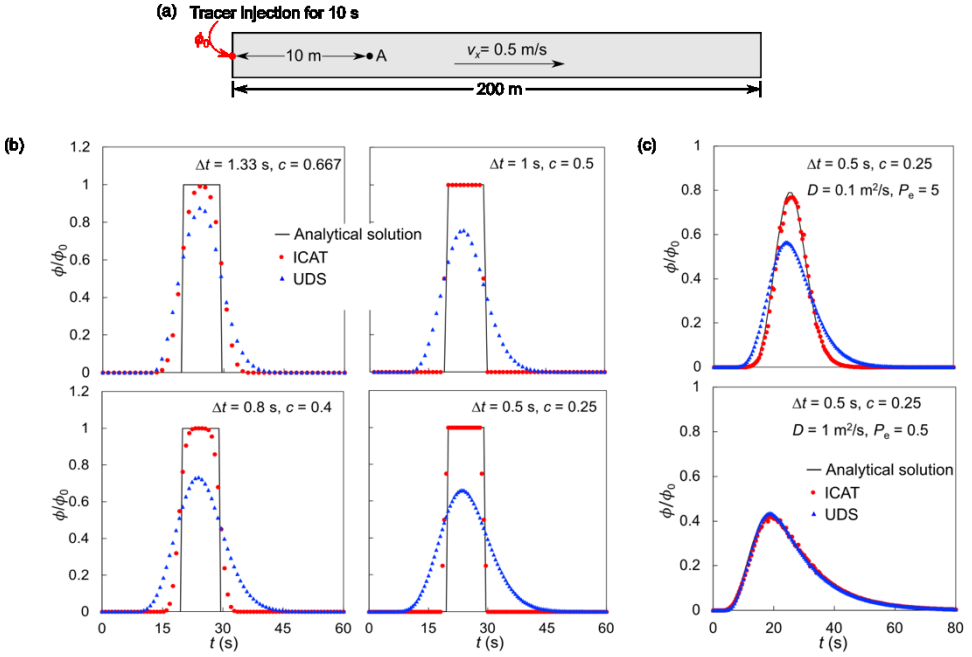

Figure 4: Comparison of tracer transport in a 1D model between the analytical solution and numerical results. (a) Diagram of the 1D model with uniform flow velocity. The model is 200 m in length and is uniformly discretized into 1 m-long cells. The tracer is injected at the left boundary for 10 s at a constant concentration ϕ_0. (b) The evolution of relative concentration at point A under different Courant numbers, solved by the three methods. (c) The evolution of relative concentration at point A under different Peclet numbers.

3.2 Transport of a scalar in a 2D model

Versteeg and Malalasekera (2007) examined the transport of a scalar in a 2D domain where the velocity field is uniform and parallel to the diagonal (O-O') across the grid (Fig. 5(a)). The boundary conditions for the scalar are $\phi_0 = 0$ along the left and bottom boundaries, and $\phi_0 = 100$ on the right and top boundaries. Versteeg and Malalasekera (2007) considered a pure advection scenario and calculated the distribution of ϕ along the diagonal X-X' under steady state using UDS and QUICK schemes (Fig. 5(b)). In this test case, we use ICAT to simulate the same situation and the results from ICAT are compared with results from UDS and QUICK.

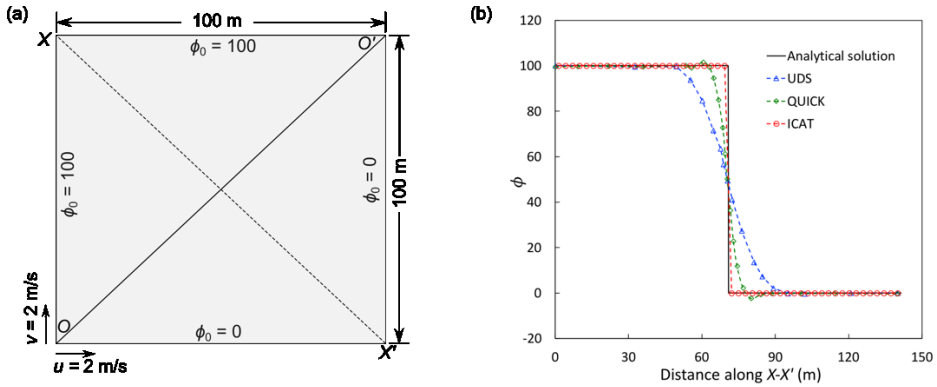

Figure 5: Comparison of different numerical schemes for the scalar distribution in a 2D model. (a) Diagram of the 2D model with uniform flow velocity. The horizontal and vertical velocities are 2 m/s. Mesh resolution is 2 m in both the horizontal and vertical directions. Time step is 0.25 s. (b) Comparison of scalar distribution along diagonal *X*-*X*′ between analytical solution and numerical results from different schemes.

As the flow is parallel to *O*-*O*′, the value of ϕ should be 100 above *O*-*O*′ and 0 below *O*-*O*′ (analytical solution in Fig. 5(b)). Numerical diffusion is the most severe for UDS, and although QUICK has less severe numerical diffusion, it suffers from oscillations with unphysical values (greater than 100 or less than 0). Results from ICAT agree the best with the analytical solution. The slight discrepancy at the middle point of *X*-*X*′ is due to the mesh resolution, and can be further reduced if we refine the mesh.

4. APPLICATION OF ICAT TO IDENTIFY FLOW CHANNELS ALONG A FRACTURE

The above analyses assume uniform flow fields. However, for real-world advection-dispersion problems such as tracer transport in a fracture, the flow field is often highly heterogeneous due to nonuniform aperture distribution, and preferential flow channels may form within the fracture (Brown et al., 1998; Guo et al., 2016a; Fu et al., 2016). In fact, tracer test has been used to identify flow channels along fracture networks in unconventional reservoirs (Dverstorp et al., 1992; Guo et al., 2016b). In this section, we investigate the performance of different numerical schemes on such heterogeneous flow filed. Specifically, we simulate the transport of a conservative tracer in a fracture with a randomly generated aperture distribution, and try to identify preferential flow channels between injection and production wells through the tracer breakthrough curve at the production well.

We model a fracture with a circular shape as shown in Fig. 6(a). The radius of the fracture is 15 m, and the distance between the injection well and the production well is 10 m. We use a spatially auto-correlated aperture distribution with the correlation length = 1.5 m, mean aperture = 0.1 mm and standard deviation = 0.17 mm. The fracture is represented by a thin layer of porous medium with an equivalent porosity (Guo et al., 2016b). The permeability of the fracture is calculated according to the cubic law. To simulate tracer transport, we first inject water into the fracture to obtain a heterogeneous but steady flow field. The circulation rate is 0.1 L/min with the water dynamic viscosity = 0.5 mPa·s. Afterward, we inject a conservative tracer with a concentration of ϕ_0 through the injection well for 1000 s and monitor the tracer concentration at the production well. The hydrodynamic dispersion coefficient of the fracture is assumed to be constant and equals 1×10^{-7} m^2/s (Zhou et al., 2018).

Five main preferential flow channels connecting the injection and production wells are visually identified in the flow field (Fig. 6(b)). Since the flow distances and velocities are different among these channels, tracers will arrive at the production well at different times, leading to multiple local peaks on the breakthrough curve at the production well. Therefore, we can characterize the preferential flow channels through the arrival times and magnitudes of the peaks on the breakthrough curve.

Fig. 6(c) compares the tracer breakthrough curves at the production well obtained from ICAT and UDS. Five peaks are resolved on the breakthrough curve from ICAT. By further analyzing the tracer transport process simulated by ICAT, we find that flow channels 1, 2, 3, 4 and 5 each correspond to a peak on the breakthrough curve. Because the numerical diffusion is more severe in the results from UDS than that from ICAT, the breakthrough curve from UDS indicates an earlier breakthrough time and a smaller magnitude for the first peak. Peaks for channels 2, 3, 4 and 5 are smeared and cannot be identified. Compared with UDS, ICAT reduces the numerical diffusion in the simulation results and the preferential flow channels in the flow field can be better resolved from the breakthrough curve.

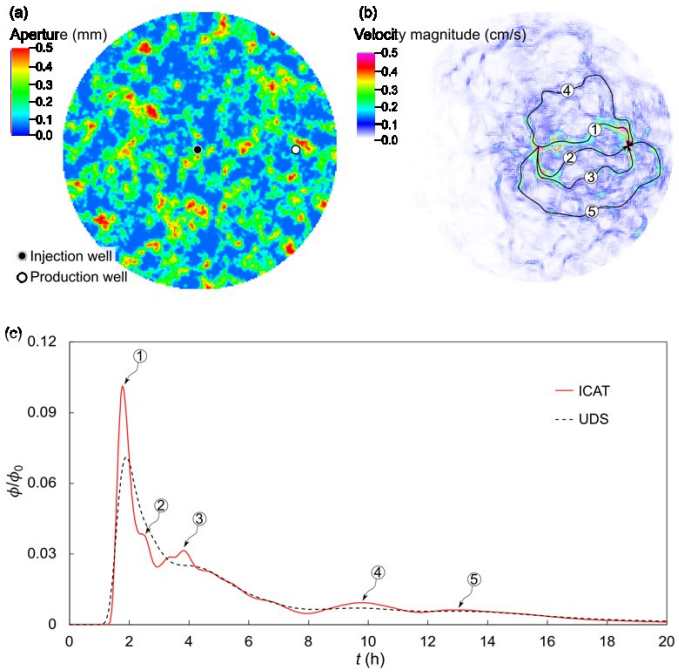

Figure 6: Tracer transport in a fracture with spatially correlated, heterogeneous aperture distribution. (a) The heterogeneous aperture distribution in the fracture. Mesh resolution is 0.15 m. (b) Velocity magnitude in the fracture at steady state. (c) Comparison of the breakthrough curves at the production well obtained from ICAT and UDS.

5. CONCLUSIONS

An accurate and robust advection-dispersion scheme is essential for the modeling of many fluid dynamics problems. We propose a new scheme, named Intra-Cell Advection Tracking (ICAT), to minimize numerical diffusion as well as preserve stability and monotonicity for advection-dispersion simulation. With the new scheme, numerical diffusion caused by truncation error and flow field-to-grid skewness can be substantially reduced or even eliminated. The efficacy of the new scheme is demonstrated through several numerical examples involving 1D and 2D flow, as well as comparison with other schemes.

The transport process of a conservative tracer in a fracture with random aperture distribution is simulated with ICAT. Discrete flow channels in the fracture are correctly identified from the tracer breakthrough curve, for both structured and unstructured mesh scenarios. Compared with some other numerical schemes, ICAT is less sensitive to mesh geometry since the numerical diffusion caused by flow filed-to-grid skewness is reduced.

ACKNOWLEDGEMENT

This material was based upon work supported by the U.S. Department of Energy, Office of Energy Efficiency and Renewable Energy (EERE), Office of Technology Development, Geothermal Technologies Office, under Award Number DE-AC52-07NA27344 with LLNL. Publication releases for this manuscript are under LLNL-CONF-766468. The United States Government retains, and the publisher, by accepting the article for publication, acknowledges that the United States Government retains a non-exclusive, paid-up, irrevocable, world-wide license to publish or reproduce the published form of this manuscript, or allow others to do so, for United States Government purposes. The research supporting this work took place in whole or in part at the Sanford Underground Research Facility in Lead, South Dakota. The assistance of the Sanford Underground Research Facility and its personnel in providing physical access and general logistical and technical support is acknowledged.

REFERENCES

Arampatzis, G., and Assimacopoulos, D.: Treatment of numerical diffusion in strong convective flows, *Int. J. Numer. Meth. Fluids*, **18**, (1994), 313-331.

Brasseur, G.P., and Jacob, D.J.: Modeling of atmospheric chemistry, Cambridge University Press, Cambridge (2017).

Brown, S., Caprihan, A., and Hardy, R.: Experimental observation of fluid flow channels in a single fracture, *J. Geophys. Res.: Solid Earth*, **103**, (1998), 5125-5132.

Calo, V.M., Brasher, N.F., Bazilevs, Y., and Hughes, T.J.R.: Multiphysics model for blood flow and drug transport with application to patient-specific coronary artery flow, *Comput. Mech.*, **43**, (2008), 161-177.

Courant, R., Friedrichs, K., and Lewy, H.: Über die partiellen Differenzengleichungen der mathematischen Physik, *Math. Ann.*, **100**, (1928), 32-74.

Dverstorp, B., Andersson, J., and Nordqvist, W.: Discrete fracture network interpretation of field tracer migration in sparsely fractured rock, *Water Resour. Res.*, **28**, (1992), 2327-2343.

Fu, P.C., Hao, Y., Walsh, S.D.C., and Carrigan, C.R.: Thermal drawdown-induced flow channeling in fractured geothermal reservoirs, *Rock Mech. Rock Eng.*, **49**, (2016), 1001-1024.

Gross, E.S., Koseff, J.R., and Monismith, S.G.: Evaluation of advective schemes for estuarine salinity simulations, *J. Hydraul. Eng.*, **125**, (1999), 32-46.

Guo, B., Fu, P.C., Hao, Y., Peters, C.A., and Carrigan, C.R.: Thermal drawdown-induced flow channeling in a single fracture in EGS, *Geothermics*, **61**, (2016a), 46-62.

Guo, B., Fu, P.C., Hao, Y., and Carrigan, C.R.: Investigating the possibility of using tracer tests for early identification of EGS reservoirs prone to flow channeling, in: 41st Stanford Geothermal Workshop, Stanford University, Stanford, CA (2016b).

Hawkins, A.J., Fox, D.B., Becker, M.W., and Tester, J.W.: Measurement and simulation of heat exchange in fractured bedrock using inert and thermally degrading tracers, *Water Resour. Res.*, **53**, (2017), 1210-1230.

Kumar, A., Jaiswal, D.K., and Kumar, N.: Analytical solutions to one-dimensional advection-diffusion equation with variable coefficients in semi-infinite media, *J. Hydrol.*, **380**, (2010), 330-337.

Lax, P.D.: Weak solutions of nonlinear equations and their numerical computation, *Comm. Pure Appl. Math.*, **7**, (1954), 159-193.

Lax, P.D., and Wendroff, B.: Systems of conservation laws, *Comm. Pure and Appl. Math.*, **13**, (1960), 217-237.

Leonard, B.P.: A stable and accurate convective modelling procedure based on quadratic upstream interpolation, *Comput. Methods Appl. Mech. Engrg.*, **19**, (1979), 59-98.

Marshall, J. Shuckburgh, E., Jones, H., and Hill, C.: Estimates and implications of surface eddy diffusivity in the southern ocean derived from tracer transport, *J. Phys. Oceanogr.*, **36**, (2006), 1806-1821.

Patankar,S.V.: Numerical heat transfer and fluid flow, Hemisphere Publishing Corporation, Washington, DC (1980).

Pontrelli, G., and de Monte, F.: Mass diffusion through two-layer porous media: an application to the drug-eluting stent, *Int. J. Heat Mass Transf.*, **50**, (2007), 3658-3669.

Roe, P.L.: Characteristic-based schemes for the Euler equations, *Ann. Rev. Fluid Mech.*, **18**, (1986), 337-365.

Rood, R.B.: Numerical advection algorithms and their role in atmospheric transport and chemistry models, *Rev. Geophys.*, **25**, (1987), 71-100.

Smolarkiewicz, P.K.: A fully multidimensional positive definite advection transport algorithm with small implicit diffusion, *J. Comput. Phys.*, **54**, (1984), 325-362.

Tang, D.H., Frind, E.O., and Sudicky, E.A.: Contaminant transport in fractured porous media: Analytical solution for a single fracture, *Water Resour. Res.*, **17**, (1981), 555-564.

van Leer, B.: Toward the ultimate conservative difference scheme IV: A new approach to numerical convection, *J. Comp. Phys.*, **23**, (1977), 276-299.

Versteeg, H.K., and Malalasekera, W.: An introduction to computational fluid dynamics the finite volume method (2nd edition), Longman Scientific & Technical, New York (2007).

Zhou, Q.L., Oldenburg, C.M., Kneafsey, T.J., and EGS Collab Team: Modeling transport of multiple tracers in hydraulic fractures at the EGS Collab test site, in: 43rd Stanford Geothermal Workshop, Stanford, California, U.S. (2018).